IEEE Access
Multidisciplinary | Rapid Review | Open Access Journal

SPECIAL SECTION ON MULTI-FUNCTION RF COMPONENTS FOR CURRENT AND FUTURE 5G WIRELESS COMMUNICATIONS

Received January 3, 2018, accepted January 31, 2018, date of publication February 5, 2018, date of current version March 19, 2018.

Digital Object Identifier 10.1109/ACCESS.2018.2801816

Dual-Band Filtering Balanced-to-Unbalanced Impedance-Transforming Power Divider With High Frequency Ratio and Arbitrary Power Division

ZHENG ZHUANG[1], YONGLE WU[2], (Senior Member, IEEE), MENGDAN KONG[1], WEIMIN WANG[1], AND YUANAN LIU[1]

[1]Beijing Key Laboratory of Work Safety Intelligent Monitoring, Department of Electronic Engineering, Beijing University of Posts and Telecommunications, Beijing 100876, China

[2]State Key Laboratory of Information Photonics and Optical Communications, School of Electronic Engineering, Beijing University of Posts and Telecommunications, Beijing 100876, China

Corresponding author: Yongle Wu (wuyongle138@gmail.com)

This work was supported in part by the National Key Basic Research Program of China (973 Program) under Grant 2014CB339900, in part by the National Natural Science Foundation of China under Grant 61671084 and Grant 61422103, in part by the State Key Laboratory of Information Photonics and Optical Communications, Beijing University of Posts and Telecommunications, China, and in part by the Young Elite Scientists Sponsorship Program by CAST under Grant YESS20150118.

ABSTRACT This paper presents a novel dual-band filtering balanced-to-unbalanced impedance-transforming out-of-phase power divider using a simple admittance inverter with an extreme high frequency ratio and arbitrary power division, which is composed of stepped-impedance transmission lines. Based on the traditional transmission-line theory and *ABCD/Y* matrix, the closed-formed analytical equations and complete design procedure are derived and provided for the filtering differential-mode transmission with high frequency ratio and good dual-band common-mode suppression. For demonstration, a designed prototype operating at 1 and 6.4 GHz are simulated, fabricated, and measured. The measured results agree well with the EM simulation perfectly.

INDEX TERMS Arbitrary power division, dual-band, filtering, balanced-to-unbalanced, power divider, and high frequency ratio.

I. INTRODUCTION

With the increasing demands of modern wireless communication systems, much attention has been paid into the multifunctional passive/active radio frequency (RF) components for reduced size and low cost [1]–[4]. Furthermore, the electromagnetic interference noise similarly plays a very important role on the performance of overall systems, especially in high-sensitive network [5], leading to a mass of investigations about balanced components including balanced filter [1], [6], power divider [7], antenna [8], diplexer [9], and amplifier [10], etc.

As a key component in front end of radio frequency (RF) system, balanced-to-unbalanced power dividers (BTUPDs) with out-of-phase/in-phase output are also extensively investigated recently to connect with the single-ended and balanced circuit simultaneously without undesired common-mode signals. In [11], a compact BTUPD using three cascaded coupled lines is reported. For further expanding the bandwidth for common-mode suppression, an additional quarter-wavelength open stub is introduced [12]. Additionally, the phase inverter [13] and 180° coupled-line section [14] achieve an in-phase output between two single-ended ports, respectively. Based on the conventional *Y*-matrix transformation, a generalized BTUPD with arbitrary power ratio is established in [15]. Above all, various BTUPDs with different performances have been designed, but the filtering integration with high frequency selectivity is not considered. In order to reject undesired signals in RF/microwave front end, a narrowband BTUPD with filtering function is proposed by using open- and short-circuit stubs [16]. In [17], the modified two-port coupled lines with open-circuit terminations are used to replace the traditional quarter-wavelength TLs for an enhanced bandwidth. For an in-phase output and filtering integration, the two-port coupled-line structure with short-circuited termination and π-shaped network are employed [18].

To support a multi-channel concurrent communication systems including 2G to 5G, the dual-/multi-band balanced components should be widely developed besides narrow/wide-band operation. Unfortunately, there are few reported works about dual-/multi-band BTUPDs so far. By using two dual-band 90° phase shifters, a dual-band BTU PD is designed with inherent impedance transformation [19]. Moreover, a dual-band filtering BTUPD is proposed based on two coupled ring resonators for high frequency selectivity [20], but their bandwidths are very narrow. In [21], the dual-band filtering response is implemented though embedding π-shaped networks with short-circuited stubs, resulting in an enhanced dual-band operating bandwidth. Nevertheless, the current reported dual-band circuits are limited to a low frequency ratio and equal power division in general.

In this paper, a brand-new dual-band filtering balanced-to-unbalanced impedance-transforming power divider (FBTUITPD) with extreme high frequency ratio and arbitrary power division is proposed, which is comprised of six admittance inverters using stepped-impedance transmission lines and a single resistor. The designed admittance inverter can achieve dual-band filtering response with two in-band transmission poles, while the single resistor is utilized to generate a good isolation between two single-ended output ports. Based on the traditional transmission-line theory and *ABCD/Y* matrix, the closed-formed analytical equations and complete design procedure are provided for realizing the following advantages: 1) dual-band filtering operation with high frequency ratio; 2) excellent differential-mode transmission with arbitrary power division; 3) good common-mode suppression; 4) inherent impedance transformation; 5) simple circuit structure.

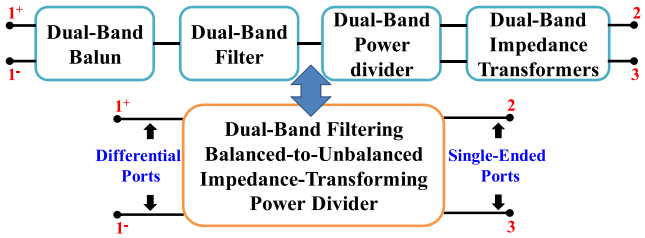

FIGURE 1. The circuit model of the proposed dual-band filtering balanced-to-unbalanced impedance-transforming power divider.

II. THEORY AND DESIGN OF FBTUITPD

Fig. 1 shows the circuit model of the proposed dual-band FBTUITPD with extreme high frequency ratio including one differential input port 1 (ports 1^+ and 1^-), and two single-ended output ports 2 and 3, which is equivalent to four cascaded dual-band balun, filter, impedance transformer, and power divider. Hereinto, the standard S-parameters ($S_{\rm std}$) in Fig. 1 can be defined as

$$S_{std} = \begin{bmatrix} S_{1^+1^+} & S_{1^+1^-} & S_{1^+2} & S_{1^+3} \\ S_{1^-1^+} & S_{1^-1^-} & S_{1^-2} & S_{1^-3} \\ S_{21^+} & S_{21^-} & S_{22} & S_{23} \\ S_{31^+} & S_{31^-} & S_{32} & S_{33} \end{bmatrix}. \tag{1}$$

The transformed relation between standard and mixed-mode S-parameters can be written as [22]

$$S_{mm} = MS_{std}M^{-1}, \tag{2a}$$

and

$$M = \frac{1}{\sqrt{2}} \begin{bmatrix} 1 & -1 & 0 & 0 \\ 1 & 1 & 0 & 0 \\ 0 & 0 & \sqrt{2} & 0 \\ 0 & 0 & 0 & \sqrt{2} \end{bmatrix}. \tag{2b}$$

Based on (1) and (2), the mixed-mode S-parameters ($S_{\rm mm}$) of the differential circuit can be derived as

$$S_{mm} = \begin{bmatrix} S_{dd11} & S_{dc11} & S_{ds12} & S_{ds13} \\ S_{cd11} & S_{cc11} & S_{cs12} & S_{cs13} \\ S_{sd21} & S_{sc21} & S_{ss22} & S_{ss23} \\ S_{sd31} & S_{sc31} & S_{ss32} & S_{ss33} \end{bmatrix}, \tag{3a}$$

and

$$\begin{cases} S_{dd11} = (S_{1^+1^+} - S_{1^+1^-} - S_{1^-1^+} + S_{1^-1^-})/2 \\ S_{cc11} = (S_{1^+1^+} + S_{1^+1^-} + S_{1^-1^+} + S_{1^-1^-})/2 \\ S_{cd11} = (S_{1^+1^+} - S_{1^+1^-} + S_{1^-1^+} - S_{1^-1^-})/2 \\ S_{dc11} = (S_{1^+1^+} + S_{1^+1^-} - S_{1^-1^+} - S_{1^-1^-})/2, \end{cases} \tag{3b}$$

$$\begin{cases} S_{sdn1} = (S_{n1^+} - S_{n1^-})/\sqrt{2} \\ S_{ds1n} = (S_{1^+n} - S_{1^-n})/\sqrt{2} \\ S_{scn1} = (S_{n1^+} + S_{n1^-})/\sqrt{2} \\ S_{cs1n} = (S_{1^+n} + S_{1^-n})/\sqrt{2}, \end{cases} \tag{3c}$$

$$S_{ssnp} = S_{np}, \tag{3d}$$

where $n, p = 2, 3$, and the subscripts d, c, and s represent the differential-mode, common-mode, and single-ended ports, respectively. As shown in Fig. 2(a), the circuit configuration for a conventional BTUPD consists of six transmission-line (TL) sections and a single resistor. Expanding from the conventional unequal BTUPD in [15], a more generalized BTUPD with impedance-transforming function and arbitrary power division is derived based on Y-matrix transformation as

$$\begin{cases} Z_1 = \sqrt{R_S R_L}\sqrt{\dfrac{1+k^2}{2}} \\ Z_2 = \sqrt{R_S R_L}\sqrt{\dfrac{1+k^2}{2k^2}} \\ Z_4 = \sqrt{\left(1+\dfrac{1}{k^2}\right)RR_L} \\ Z_5 = \sqrt{\left(1+k^2\right)RR_L}, \end{cases} \tag{4}$$

where k^2 is the power-dividing ratio ($k^2 = |S_{\rm sd31}/S_{\rm sd21}|^2$). In order to further achieve a dual-band operation with extreme high frequency ratio, a symmetrical stepped-impedance admittance inverter with the same electrical length $\theta$is utilized to replace the conventional quarter-wavelength TL, as

illustrated in Fig. 2(b). Thus, the following condition for the proposed dual-band admittance inverter should satisfy:

$$\begin{bmatrix} A & B \\ C & D \end{bmatrix} = \begin{bmatrix} 0 & \pm Z_i \\ \pm 1/Z_i & 0 \end{bmatrix}, \tag{5}$$

where Z_i is the corresponding characteristic impedance of the TL for the conventional BTUPD in (4) and i =1 to 5. Based on the traditional TL theory [23], the *ABCD*-matrix of the proposed dual-band admittance inverter can be written as

$$\begin{bmatrix} A & B \\ C & D \end{bmatrix} = \begin{bmatrix} \cos\theta & jZ_{i1}\sin\theta \\ j\dfrac{\sin\theta}{Z_{i1}} & \cos\theta \end{bmatrix} \begin{bmatrix} \cos\theta & jZ_{i2}\sin\theta \\ j\dfrac{\sin\theta}{Z_{i2}} & \cos\theta \end{bmatrix} \cdot \begin{bmatrix} \cos\theta & jZ_{i1}\sin\theta \\ j\dfrac{\sin\theta}{Z_{i1}} & \cos\theta \end{bmatrix}, \tag{6a}$$

where

$$\begin{cases} A = \dfrac{\cos\theta\left[Z_{i1}Z_{i2}\cos^2\theta - \left(Z_{i1}^2 + Z_{i1}Z_{i2} + Z_{i2}^2\right)\sin^2\theta\right]}{Z_{i1}Z_{i2}} \\ B = \dfrac{j\sin\theta\left[Z_{i2}\left(2Z_{i1} + Z_{i2}\right)\cos^2\theta - Z_{i1}^2\sin^2\theta\right]}{Z_{i2}} \\ C = \dfrac{j\sin\theta\left[Z_{i1}\left(Z_{i1} + 2Z_{i2}\right)\cos^2\theta - Z_{i2}^2\sin^2\theta\right]}{Z_{i1}^2Z_{i2}} \\ D = \dfrac{\cos\theta\left[Z_{i1}Z_{i2}\cos^2\theta - \left(Z_{i1}^2 + Z_{i1}Z_{i2} + Z_{i2}^2\right)\sin^2\theta\right]}{Z_{i1}Z_{i2}}. \end{cases} \tag{6b}$$

Due to the symmetrical stepped-impedance admittance inverter by using TL, only A and B of elements of the *ABCD* matrix from (5) and (6) need to be considered into

$$\begin{cases} A(f_1) = A(f_2) = 0 \\ B(f_1) = B(f_2) = \pm Z_i. \end{cases} \tag{7}$$

Then using simultaneous equations (6) and (7), the circuit parameters of the proposed FBTUITPD can be deduced as

$$\begin{cases} Z_{i1} = \csc(2\theta)\dfrac{2Z_i\cos\theta + \sqrt{2Z_i^2\left[\cos(2\theta) + \cos(4\theta)\right]}}{2} \\ Z_{i2} = Z_i\csc\theta - Z_{i1} \\ \theta = \dfrac{\pi}{1+a}, \end{cases} \tag{8}$$

where a is the dual-band frequency ratio (= f_2/f_1). Since the quantity under the square root sign in (8) for $[\cos(2\theta) + \cos(4\theta)]$ should be equal or greater than 0, the frequency ratio a needs to be equal or greater than 5 for a real solution. It is worth noting that the proposed admittance inverter will become a conventional quarter-wavelength TL in Fig. 2(a) when a is 5. From the above, the closed-formed analytical equations have been derived and given in (4) and (8) based on the traditional TL theory and *ABCD*/*Y* matrix. Fig. 3(a) shows the *S*-parameter of the dual-band admittance inverter with different frequency ratio a. It is clear that the large frequency ratio would attenuate the in-band return loss, but still maintain 15-dB level at least. As illustrated in Fig. 3(b), the characteristic impedances Z_{i1} increases as the increasing of a, while the Z_{i2} would decrease. Therefore, the frequency ratio

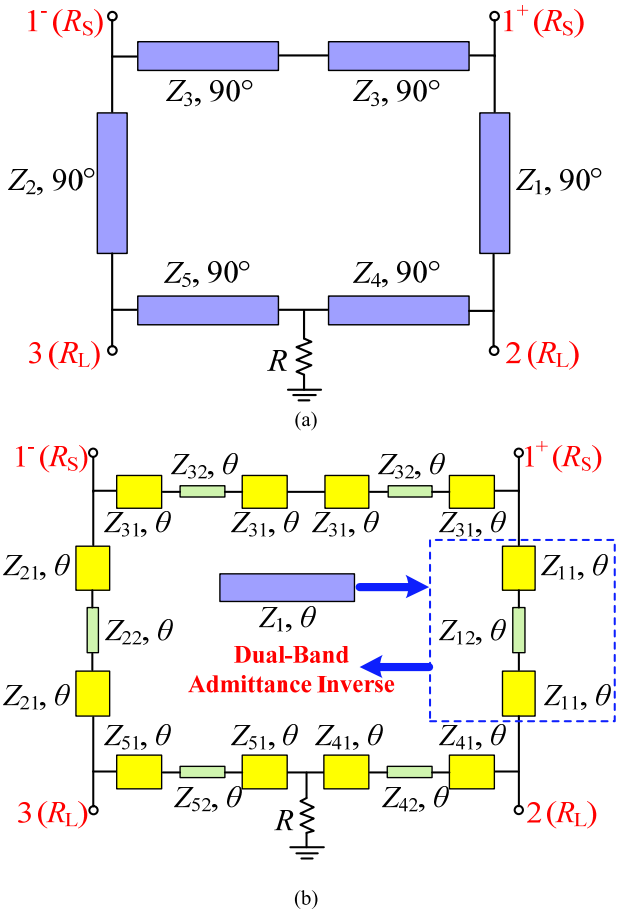

FIGURE 2. The circuit configuration of the (a) conventional and the (b) proposed balanced-to-unbalanced power divider.

TABLE 1. The calculated characteristic impedances of the 50 Ω-to-50 Ω FBTUITPD with different free variables in Fig. 4.

Free variables	Z_{11} (Ω)	Z_{12} (Ω)	Z_{31} (Ω)	Z_{32} (Ω)	Z_{41} (Ω)	Z_{42} (Ω)
Z_3=50 Ω, R=25 Ω	95.10	26.29	95.10	26.29	95.10	26.29
Z_3=50 Ω, R=56.25 Ω	95.10	26.29	95.10	26.29	142.65	39.43
Z_3=75 Ω, R=25 Ω	95.10	26.29	142.65	39.43	95.10	26.29
Z_3=75 Ω, R=56.25 Ω	95.10	26.29	142.65	39.43	142.65	39.43

needs to be limited to 10 in general for effective fabrication. We assume that the values of Z_i and f_1 is 50 Ω and 1 GHz in Fig. 3, respectively, and other parameters can be calculated by (8) based on the prescriptive frequency ratio.

Combining with (4) and (8), the proposed dual-band admittance inverter can be employed to replace the conventional quarter-wavelength TL for implementing a dual-band FBTUITPD. In this work, Z_2 and R are set as free variables. Thus, according to the specified terminal impedance (R_S, R_L), resistor R, power-dividing ratio k^2, and frequency ratio a, the proposed dual-band FBTUITPD can be constructed by (4) and (8). The influences of free variables on the circuit performance are discussed in the following Section III.

III. CASES ANALYSIS OF FBTUITPD

A. 50 Ω-TO-50 Ω MATCHING CASE

Based on the above theory and circuit structure, the 50 Ω-to-50 Ω matching is only a special case. We arbitrarily

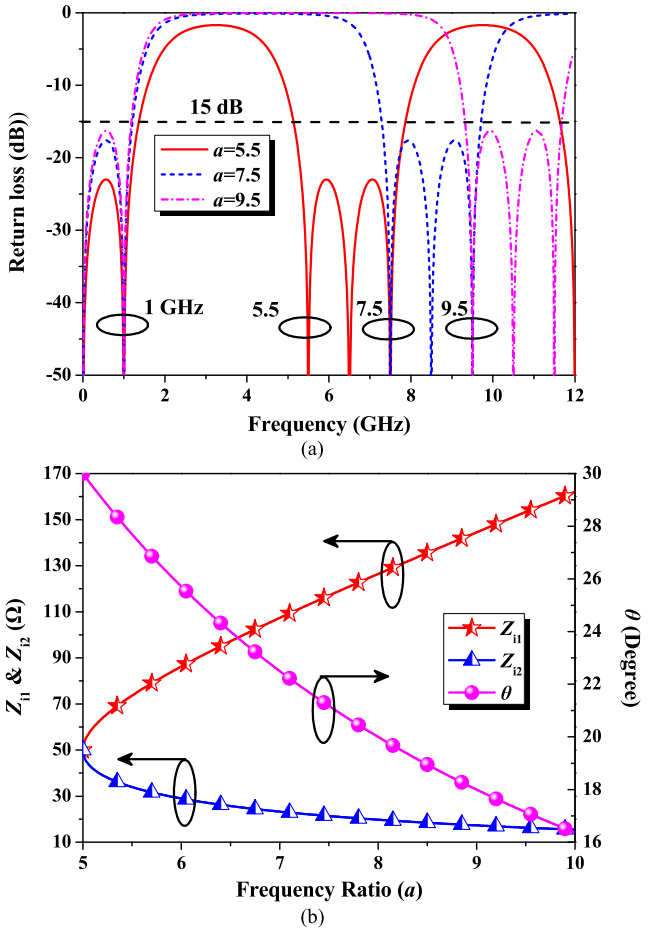

FIGURE 3. (a) The ideal simulated results of the dual-band admittance inverter with different frequency ratio a. (b) The relation between frequency ratio a and characteristic impedances (Z_{i1}, Z_{i2}), electrical length θ and.

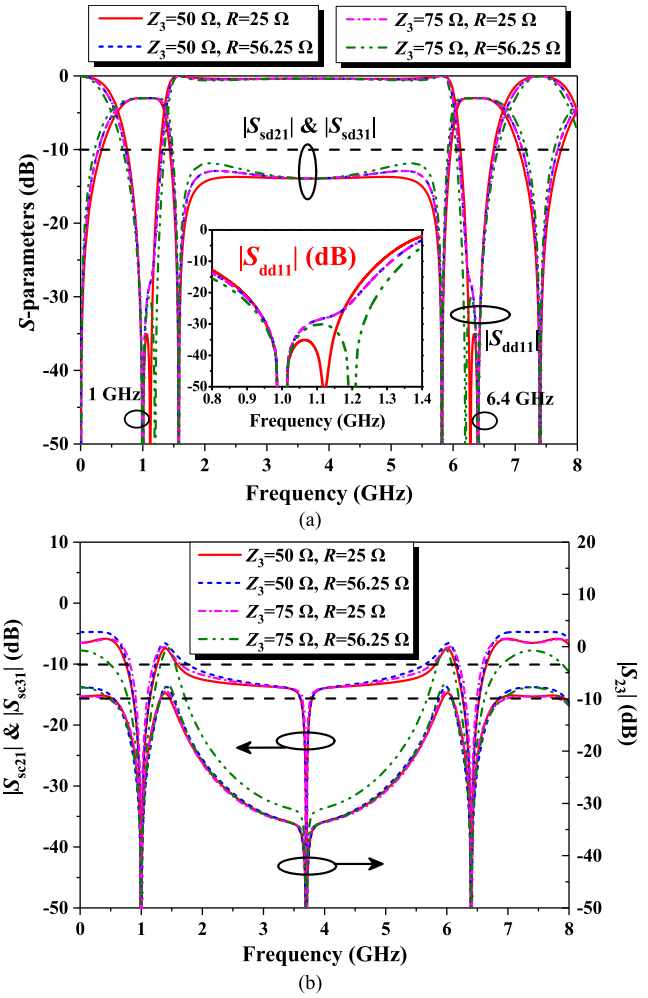

FIGURE 4. The ideal results of the proposed FBTUITPD with 50 Ω-to-50 Ω matching. (a) Differential-mode responses. (b) Common-mode responses and isolation.

assume that f_1 and a are the 1 GHz and 6.4 within the available range in Fig. 3, respectively. Thus, the electrical length θ is 24.32° by (8). For simplifying the parameter analysis, k is set as 1. By using (4) and (8) with the different free variables (Z_2, R), the circuit parameters can be calculated and shown in TABLE 1. Note that $Z_1 = Z_2$, $Z_4 = Z_5$ when $k = 1$. As shown in Fig. 4, two in-band transmission poles will be generated via the proper values of Z_3 and Z_4 (determined by R) when the port impedances are all the 50 Ω. Moreover, large Z_3 and R would expand the bandwidth of differential- and common-mode bandwidth, whereas the bandwidth of isolation is reduced. Therefore, the values of Z_3 and R have to be tradeoff between differential-/common-mode bandwidth and isolation.

B. IMPEDANCE-TRANSFORMING CASE

The proposed circuit configuration can achieve an inherent impedance-transforming function. As depicted in Fig. 5, a 50 Ω-to-75 Ω FBTUITPD at 1 and 6.4 GHz with different free variables (Z_3, R) is designed and simulated. To simplify the parameter analysis, k is set as 1. For the different port impedances, the two in-band transmission poles would be realized with different values of Z_3 and Z_4 (determined by R). Furthermore, the bandwidth of differential-mode transmission improves with the increasing of Z_3 and R, while the bandwidth of common-mode suppression would decrease. Additionally, Fig. 6 plots the S-parameters curves of the proposed FBTUITPD versus different port impedances at the case of two in-band transmission poles so as to verify the effective circuit structure and design method. By using (4) and (8), the corresponding circuit parameters for implementing Figs. 5 and 6 are shown in TABLE 2 and TABLE 3, respectively. Moreover, all the electrical length θ is 24.32° by (8). Note that the non 50 Ω ports can be effectively measured by using de-embedding method in [2].

C. UNEQUAL POWER-DIVIDING CASE

In order to perform the arbitrary power division, a 50 Ω-to-50 Ω FBTUITPD at 1 and 6.4 GHz with different power-dividing ratio k^2 from 1 to 3 is designed and simulated in Fig. 7. For the realizable range of characteristic

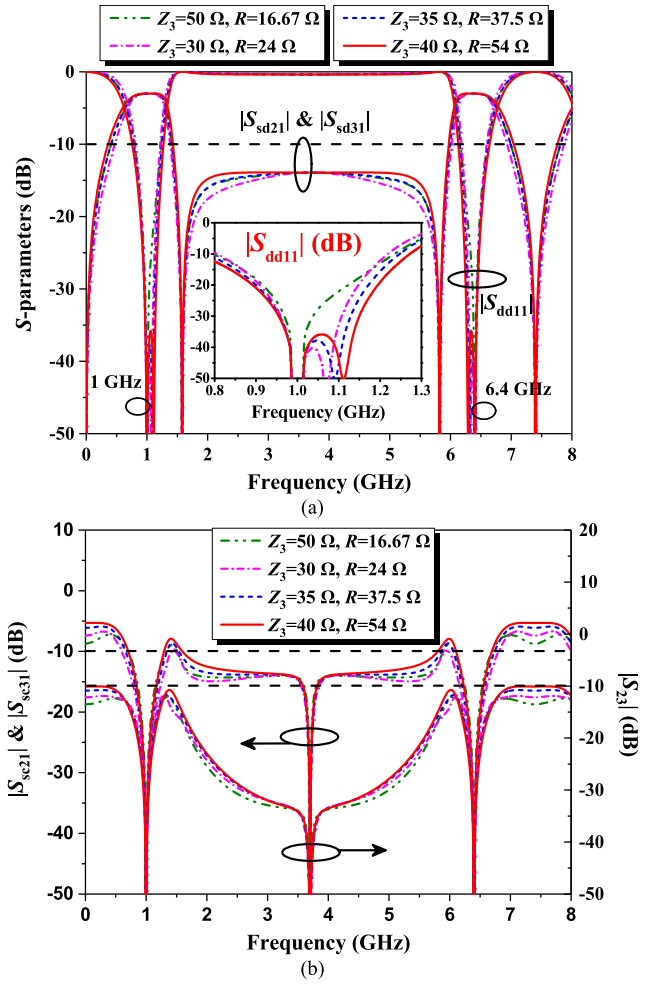

FIGURE 5. The ideal results of the proposed FBTUITPD with 50 Ω-to-75 Ω transformations. (a) Differential-mode responses. (b) Common-mode responses and isolation.

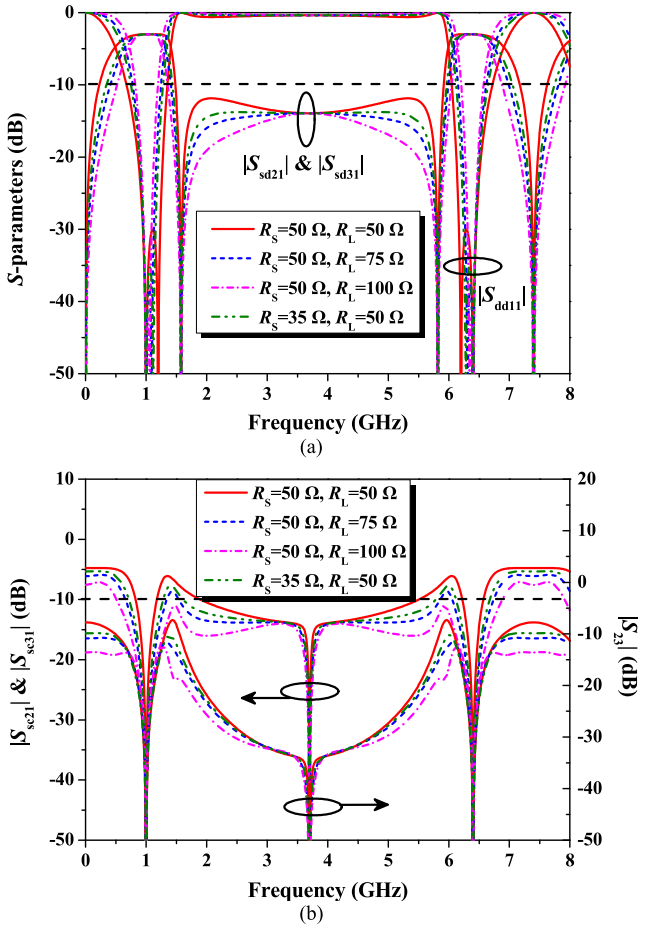

FIGURE 6. The ideal results of the proposed FBTUITPD with different port impedances. (a) Differential-mode responses. (b) Common-mode responses and isolation.

impedances, the resistor R is set at 25 Ω. For achieving two in-band TPs, the values of Z_3 are selected as 50 Ω, 46 Ω, and 43 Ω, respectively, for different k^2 from 1 to 3. Thus, all circuit parameters can be determined and calculated in TABLE 4 by using (4) and (8). Besides, all the electrical length θ is 24.32° by (8). From Fig. 7, it's obvious that the proposed dual-band FBTUITPD can effectively carry out arbitrary power division.

D. DESIGN PROCEDURE

According to the aforementioned theory and analysis, the complete design procedure for the proposed dual-band FBTUITPD is summarized as follows:

1) Specify the desired dual-band operating frequency (f_1, f_2), power-dividing ratio k^2, and terminated impedances (R_S, R_L). In this work, the dual-band operation is adapted for extreme high frequency ratio $a(\geq 5)$. Thus, the equivalent dual-band admittance inverter would not cause a big circuit size comparing with the conventional BTUPD, due to the electrical length of each TL below 30° by (8).
2) By using (4) and (8), calculate the circuit parameters of the first and second dual-band stepped-impedance admittance inverters including $Z_{11}, Z_{12}, Z_{21}, Z_{22}$, and θ.
3) In order to achieve two in-band transmission poles with higher frequency selectivity, Z_3 and R should be selected properly according to the analysis of Figs. 4 and 5. For the general 50 Ω terminated impedances and equal power division, the values of Z_3, Z_4, and Z_5 should be identical.
4) Then, based on the selected Z_3 and R, the other parameters including Z_{31}, Z_{32}, Z_{41}, Z_{42}, Z_{51}, and Z_{52} can be determined by (4) and (8).

Finally, construct the proposed circuit model shown in Fig. 2(b).

IV. SIMULATED AND MEASURED RESULTS

For further demonstration, a dual-band equal FBTUITPD prototype with 50 Ω-to-50 Ω matching at 1 and 6.4 GHz shown in Fig. 8 is designed, fabricated and measured on the RO4350B substrate with a relative permittivity of 3.66, a thickness of 0.762 mm, and a loss tangent of 0.0037. In this work, free variables (Z_3, R) are selected as 50 Ω

TABLE 2. The calculated characteristic impedances of the 50 Ω-to-75 Ω FBTUITPD with different free variables in Fig. 5.

Free variables	Z_{11} (Ω)	Z_{12} (Ω)	Z_{31} (Ω)	Z_{32} (Ω)	Z_{41} (Ω)	Z_{42} (Ω)
Z_3=50 Ω, R=16.67 Ω	116.47	32.20	95.10	26.29	95.10	26.29
Z_3=30 Ω, R=24 Ω	116.47	32.20	57.06	15.78	114.12	31.55
Z_3=35 Ω, R=37.5 Ω	116.47	32.20	66.57	18.40	142.65	39.43
Z_3=40 Ω, R=54 Ω	116.47	32.20	76.08	21.03	171.18	47.32

TABLE 3. The calculated characteristic impedances of the proposed FBTUITPD with different port impedances in Fig. 6.

Free variables	Z_{11} (Ω)	Z_{12} (Ω)	Z_{31} (Ω)	Z_{32} (Ω)	Z_{41} (Ω)	Z_{42} (Ω)
R_S=50 Ω, R_L=50 Ω Z_3=75 Ω, R=56.25 Ω	95.10	26.29	142.65	39.43	142.65	39.43
R_S=50 Ω, R_L=75 Ω Z_3=35 Ω, R=37.5 Ω	116.47	32.20	66.57	18.40	142.65	39.43
R_S=50 Ω, R_L=100 Ω Z_3=25 Ω, R=28.125 Ω	134.49	37.18	44.55	13.14	142.65	39.43
R_S=35 Ω, R_L=50 Ω Z_3=30 Ω, R=36 Ω	79.57	21.99	57.06	15.78	114.12	31.55

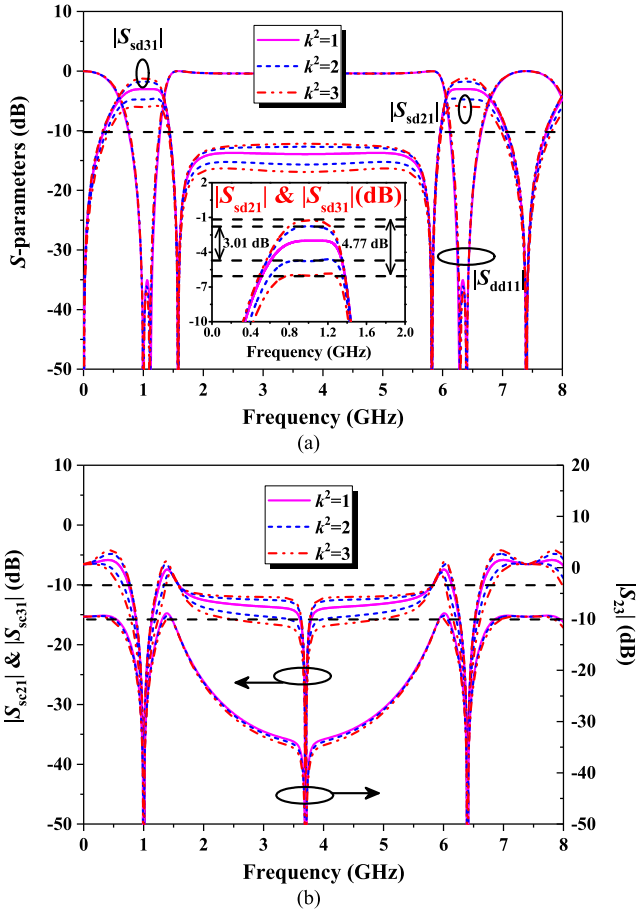

FIGURE 7. The ideal results of the proposed FBTUITPD with different power-dividing ratio. (a) Differential-mode responses. (b) Common-mode responses and isolation.

and 25 Ω for simplification, respectively. And then all circuit parameters are calculated by (4) and (8) as follows: $Z_{11} = Z_{21} = Z_{31} = Z_{41} = Z_{51} = 95.10\ \Omega$, $Z_{12} = Z_{22} =$

TABLE 4. The calculated characteristic impedances of the 50 Ω-to-50 Ω FBTUITPD with different Power-dividing Ratio in Fig. 7.

Free variables	Z_{11} (Ω)	Z_{12} (Ω)	Z_{21} (Ω)	Z_{22} (Ω)	Z_{31} (Ω)	Z_{32} (Ω)	Z_{41} (Ω)	Z_{42} (Ω)	Z_{51} (Ω)	Z_{52} (Ω)
k^2=1 Z_3=50 Ω, R=25 Ω	95.10	26.29	95.10	26.29	95.10	26.29	95.10	26.29	95.10	26.29
k^2=2 Z_3=46 Ω, R=25 Ω	116.47	32.20	82.36	22.77	87.49	24.19	82.36	22.77	116.47	32.20
k^2=3 Z_3=43 Ω, R=25 Ω	134.49	37.18	77.65	21.46	81.79	22.61	77.65	21.46	134.49	37.18

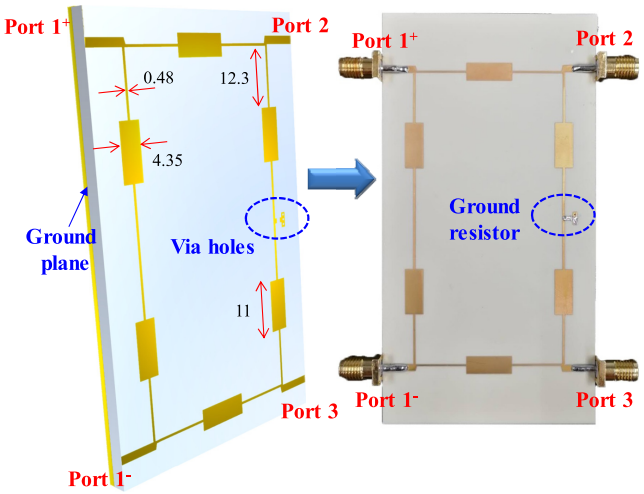

FIGURE 8. The circuit layout and photograph of the proposed dual-band FBTUITPD on the substrate of RO4350B (Unit: mm).

TABLE 5. Performance comparison of dual-band balanced-to-unbalanced power dividers.

Refs.	Operating Frequency (GHz)	RBW	CMS(dB) @f_1 & f_2	In-band TPs	IT
[19]	0.9 &1.8	11.9% & 5.9%	-22 & -17	1	Yes
[20]	2.82 & 3.22	7.9% & 6.9%	<-15 & <-15	2	No
[21]	1 & 2.2	46% & 21.8%	-15.3 & -14.7	2	No
This work	1 & 6.4	53% & 7.3%	-38.3 & -28.2	2	Yes

RBW: 10-dB Relative bandwidth; CMS: Common-mode suppression; TPs: Transmission poles; IT: Impedance Transformation.

$Z_{32} = Z_{42} = Z_{52} = 26.29\ \Omega$, $\theta = 24.32°$. The electromagnetic simulations are performed by Advanced Design System (ADS) based on the Method of Moment (MOM). Fig. 9 shows the EM simulated and measured results of the proposed dual-band FBTUITPD prototype with 50 Ω-to-50 Ω matching at 1 and 6.4 GHz. Good agreement can be observed between EM simulated and measured results.

For the first passband at 1 GHz, the relative bandwidth of the measured 10-dB differential-mode input return loss $|S_{dd11}|$ is about 58% from 0.72 to 1.3 GHz, while the differential-mode insertion loss $|S_{sd21}|$ is 3.45 dB at 1 GHz. Besides, the measured common-mode suppression $|S_{sc21}|$ is better than 10 dB from 0.75 to 1.33 GHz with the $|S_{cc11}|$ greater than -5.98 dB. In addition, the measured output matching $|S_{22}|$ is below −10 dB from 0.71 to 1.28 GHz, while the corresponding 10- dB isolation $|S_{23}|$ is ranged

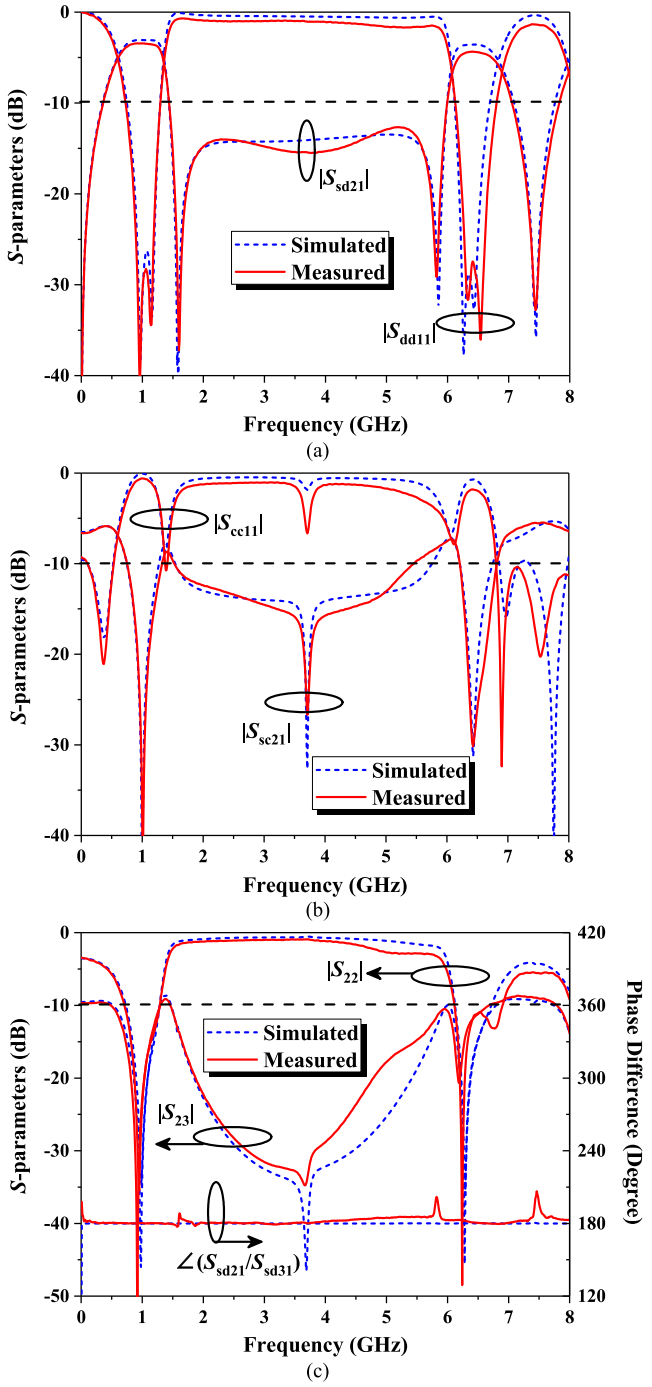

FIGURE 9. The EM simulated and measured results of the proposed dual-band FBTUITPD for (a) differential-mode responses (| S_{dd11} |, | S_{sd21} |), (b) common-mode responses (| S_{cc11} |, | S_{sc21} |), and (c) output matching, isolation (| S_{22} |, | S_{23} |), and phase difference.

from 0.49 to 1.3 GHz. The in-band phase difference is 180° ± 0.3°. Therefore, in the cases of the return losses, isolation, and common-mode suppression ($|S_{dd11}|$, $|S_{sc21}|$, $|S_{22}|$, $|S_{23}|$) < -10 dB, the operating bandwidth of the first passband is about 53% (530 MHz).

For the second passband at 6.4 GHz, the relative bandwidth of the measured 10-dB differential-mode input return loss $|S_{dd11}|$ is about 10.5% from 6.13 to 6.8 GHz, while the differential-mode insertion loss $|S_{sd21}|$ is 4.37 dB at 6.4 GHz. Moreover, the measured common-mode suppression $|S_{sc21}|$ is less than −10 dB from 6.21 to 6.75 GHz with the $|S_{cc11}|$ greater than -6 dB. Furthermore, the measured 10-dB output matching $|S_{22}|$ and isolation $|S_{23}|$ is ranged from 6.11 to 6.68 GHz. The in-band phase difference is 180° ± 3° . Thus, in the cases of the return losses, isolation, and common-mode suppression ($|S_{dd11}|$, $|S_{sc21}|$, $|S_{22}|$, $|S_{23}|$) < -10 dB, the operating bandwidth of the first passband is about 7.3% (470 MHz). Finally, the performance comparison is listed in TABLE 5. The connector losses, the effect of soldering, and manufacturing errors maybe lead to the deviations between the simulated and measured results.

V. CONCLUSION

A new and simple dual-band filtering balanced-to-unbalanced out-of-phase power divider is proposed in this paper by using equivalent stepped-impedance admittance inverter with extreme high frequency ratio, inherent impedance transformation, arbitrary power division, excellent differential-mode return loss including two in-band transmission poles, good common-mode suppression, comparable output matching and isolation. Hence, this power divider has a large potential applied in the modern wireless communication systems including 2G to 5G.

REFERENCES

[1] S.-X. Zhang, L.-L. Qiu, and Q.-X. Chu, "Multiband balanced filters with controllable bandwidths based on slotline coupling feed," *IEEE Microw. Wireless Compon. Lett.*, vol. 27, no. 11, pp. 974–976, Nov. 2017.

[2] L. Jiao *et al.*, "Design methodology for six-port equal/unequal quadrature and rat-race couplers with balanced and unbalanced ports terminated by arbitrary resistances," *IEEE Trans. Microw. Theory Techn.*, to be published. [Online]. Available: http://ieeexplore.ieee.org/document/8187723/, doi: 10.1109/TMTT.2017.2778108.

[3] R. Gómez-García, R. Loeches-Sánchez, D. Psychogiou, and D. Peroulis, "Single/multi-band Wilkinson-type power dividers with embedded transversal filtering sections and application to channelized filters," *IEEE Trans. Circuits Syst. I, Reg. Papers*, vol. 62, no. 6, pp. 1518–1527, Jun. 2015.

[4] J.-X. Xu, X. Y. Zhang, and X.-Q. Song, "High-efficiency filter-integrated class-F power amplifier based on dielectric resonator," *IEEE Microw. Wireless Compon. Lett.*, vol. 27, no. 9, pp. 827–829, Sep. 2017.

[5] H. Zhang, L. Yang, S. Wang, and J. Puukko, "Common-mode EMI noise modeling and reduction with balance technique for three-level neutral point clamped topology," *IEEE Trans. Ind. Electron.*, vol. 64, no. 9, pp. 7563–7573, Sep. 2017.

[6] W. Feng, X. Gao, W. Che, W. Yang, and Q. Xue, "High selectivity wideband balanced filters with multiple transmission zeros," *IEEE Trans. Circuits Syst. II, Exp. Briefs*, vol. 64, no. 10, pp. 1182–1186, Oct. 2017.

[7] Y. Xiao, F. Lin, H. Ma, X. Tan, and H. Sun, "A planar balanced power divider with tunable power-dividing ratio," *IEEE Trans. Microw. Theory Techn.*, vol. 65, no. 12, pp. 4871–4882, Dec. 2017.

[8] F. Sarrazin, S. Pflaum, and C. Delaveaud, "Radiation efficiency improvement of a balanced miniature IFA-inspired circular antenna," *IEEE Antennas Wireless Propag. Lett.*, vol. 16, pp. 1309–1312, 2017.

[9] Y. Zhou, H.-W. Deng, and Y. Zhao, "Compact balanced-to-balanced microstrip diplexer with high isolation and common-mode suppression," *IEEE Microw. Wireless Compon. Lett.*, vol. 24, no. 3, pp. 143–145, Mar. 2014.

[10] H. Alzaher and M. Ismail, "A CMOS fully balanced differential difference amplifier and its applications," *IEEE Trans. Circuits Syst. II, Analog Digit. Signal Process.*, vol. 48, no. 6, pp. 614–620, Jun. 2001.

[11] W. Zhang, Y. Wu, Y. Liu, F. M. Ghannouchi, and A. Hasan, "A wideband balanced-to-unbalanced coupled-line power divider," *IEEE Microw. Wireless Compon. Lett.*, vol. 26, no. 6, pp. 410–412, Jun. 2016.
[12] J. Shi, J. Lu, K. Xu, and J.-X. Chen, "A coupled-line balanced-to-single-ended out-of-phase power divider with enhanced bandwidth," *IEEE Trans. Microw. Theory Techn.*, vol. 65, no. 2, pp. 459–466, Feb. 2017.
[13] L.-S. Wu, Y.-X. Guo, L.-F. Qiu, and J.-F. Mao, "A new balanced-to-single-ended (BTSE) power divider," in *Proc. IEEE Int. Wireless Symp.*, Mar. 2014, pp. 1–4.
[14] Y. Wu, Z. Zhuang, L. Jiao, and Y. Liu, "A novel balanced-to-unbalanced complex impedance-transforming in-phase power divider," *IEEE Access*, vol. 5, pp. 16205–16213, 2017.
[15] A. N. Yadav and R. Bhattacharjee, "Balanced to unbalanced power divider with arbitrary power ratio," *IEEE Microw. Wireless Compon. Lett.*, vol. 26, no. 11, pp. 885–887, Nov. 2016.
[16] K. Xu, J. Shi, L. Lin, and J.-X. Chen, "A balanced-to-unbalanced microstrip power divider with filtering function," *IEEE Trans. Microw. Theory Techn.*, vol. 63, no. 8, pp. 2561–2569, Aug. 2015.
[17] X. Gao, W. Feng, W. Che, and Q. Xue, "Wideband balanced-to-unbalanced filtering power dividers based on coupled lines," *IEEE Trans. Microw. Theory Techn.*, vol. 65, no. 1, pp. 86–95, Jan. 2017.
[18] L. Jiao, Y. Wu, Z. Zhuang, Y. Liu, and A. A. Kishk, "Planar balanced-to-unbalanced in-phase power divider with wideband filtering response and ultra-wideband common-mode rejection," *IEEE Trans. Circuits Syst. I, Reg. Papers*, to be published. [Online]. Available: http://ieeexplore.ieee.org/document/8100623/, doi: 10.1109/TCSI.2017.2766366.
[19] W. Zhang *et al.*, "Dual-band balanced-to-unbalanced power divider with inherent impedance transformation," *Electromagnetics*, vol. 37, no. 2, pp. 127–137, Mar. 2017.
[20] W. Feng, M. Hong, and W. Che, "Dual-band balanced-to-unbalanced filtering power divider by coupled ring resonators," *Electron. Lett.*, vol. 52, no. 22, pp. 1862–1864, Oct. 2016.
[21] Z. Zhuang, Y. Wu, and Y. Liu, "Dual-band filtering out-of-phase balanced-to-single-ended power divider with enhanced bandwidth," *AEU-Int. J. Electron. Commun.*, vol. 82, pp. 341–345, Dec. 2017.
[22] W. R. Eisenstadt, B. Stengel, and B. M. Thompson, *Microwave Differential Circuit Design Using Mixed-Mode S-Parameters*. Boston, MA, USA: Artech House, 2006.
[23] D. M. Pozar, *Microwave Engineering*, 3rd ed. New York, NY, USA: Wiley, 2005.

ZHENG ZHUANG received the B.S. degree in electronic science and technology from the Beijing University of Chemical Technology, Beijing, China, in 2015. He is currently pursuing the Ph.D. degree with the Beijing University of Posts and Telecommunications.

His research interests include microwave passive components, power amplifiers, and transformation optics.

YONGLE WU (M'12–SM'15) received the B.Eng. degree in communication engineering and the Ph.D. degree in electronic engineering from the Beijing University of Posts and Telecommunications (BUPT), Beijing, China, in 2006 and 2011, respectively.

In 2010, he was a Research Assistant with the City University of Hong Kong, Kowloon, Hong Kong. In 2011, he joined BUPT, where he is currently a Full Professor with the School of Electronic Engineering. His research interests include microwave components and wireless systems design.

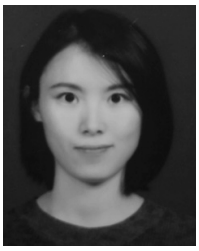

MENGDAN KONG received the B.S. degree in electronic science and technology from the Beijing University of Posts and Telecommunications, Beijing, China, in 2017, where she is currently pursuing the M.S. degree.

Her research interests include microwave passive components, metamaterial and graphene-based terahertz devices.

WEIMIN WANG received the B.S. degree in communication engineering, the M.S. degree in electromagnetic field and microwave technology, and the Ph.D. degree in electronic science and technology from the Beijing University of Posts and Telecommunications (BUPT), Beijing, China, in 1999, 2004, and 2014, respectively. In 2014, she joined BUPT, where she is currently a Lecturer with the School of Electronic Engineering. Her research interests include electromagnetic field and MIMO OTA measurement.

YUANAN LIU received the B.E., M.Eng., and Ph.D. degrees in electrical engineering from the University of Electronic Science and Technology of China, Chengdu, China, in 1984, 1989, and 1992, respectively.

In 1984, he joined the 26th Institute of Electronic Ministry of China to develop the inertia navigating system. In 1992, he began his first post-doctoral position with the EMC Laboratory, Beijing University of Posts and Telecommunications (BUPT), Beijing, China. In 1995, he started his second post-doctoral position at the Broadband Mobile Laboratory, Department of System and Computer Engineering, Carleton University, Ottawa, Canada. Since 1997, he has been a Professor with the Wireless Communication Center, College of Telecommunication Engineering, BUPT, Beijing, China, where he is involved in the development of next-generation cellular system, wireless LAN, Bluetooth application for data transmission, EMC design strategies for high speed digital system, and EMI and EMS measuring sites with low cost and high performance.